PROCEEDINGS OF SCIENCE

Dilepton Backward Rapidity Distributions

M. B. Gay Ducati[*a], **M. A. Betemps**[ab] **and E. G. de Oliveira**[a]

[a]
High Energy Physics Phenomenology Group (GFPAE),
Instituto de Física, Universidade Federal do Rio Grande do Sul,
Caixa Postal 15051, CEP 91501-970, Porto Alegre, RS, Brazil

[b]
Conjunto Agrotécnico Visconde da Graça, CAVG,
Universidade Federal de Pelotas,
Caixa Postal 460, CEP 96060-290, Pelotas, RS, Brazil

E-mail: beatriz.gay@ufrgs.br, marcos.betemps@ufrgs.br, emmanuel.deoliveira@ufrgs.br

The dilepton production at backward rapidities in pAu and pp collisions is investigated in the dipole approach, at RHIC and LHC energies. The nuclear modification ratio R_{pA} is calculated as a function of transverse momentum and of rapidity. A strong dependence of this ratio on the nuclear structure function ratio $R_{F_2} = F_2^A/F_2^p$ is found, implying that the dilepton production at backward rapidities carries information of the nuclear effects. Additionally, a comparison at RHIC energies with dilepton production at forward rapidities is provided: one of the conclusions is that the ratio R_{pA} is reduced as p_T increases at backward rapidities and reveals large x effects (for LHC, also small x), presenting the opposite behavior of the one found at forward rapidities, which evidentiates saturation effects.

DIFFRACTION 2006 – International Workshop on Diffraction in High-Energy Physics
Adamantas, Milos Island, Greece
September, 5-10 2006

[*] Speaker.

PoS(DIFF2006)053

In the most recent colliders, the hadron transverse momentum spectrum has being investigated through nuclear modification ratios relating dAu and pp collisions [1]. For forward rapidities, the transverse momentum distribution of this ratio shows a peak (called Cronin peak) at central rapidities, suppressed at more forward ones. This behavior is compatible with a Color Glass Condensate (CGC) description of the saturated regime at high energies [2]. Furthermore, the CGC analysis of the dilepton production at forward rapidities [3] implies that the Cronin effect, verified on the hadron sector (peak and suppression), should be considered as an initial state effect. Nonetheless, at backward rapidities, there is a Cronin peak in the hadrons RHIC data [4] not completely understood.

At very high energy, proton-nucleus collisions and forward rapidities, the nucleus should be described as a high density system. In this kinematical region the linear evolution equations (DGLAP [5], BFKL [6]) predict a fast growing of the number of partons, since only emission diagrams are under consideration. The non-linear contributions (recombination of partons) should reach a saturated regime at high density. These features were investigated in several works [7, 8, 9, 10]. While at forward rapidities, the saturation effects play an important role in the determination of the observables, at backward rapidities and proton-nucleus collision, the large x effects could be determinant to describe the experimental results.

In this work it is provided a study of the dilepton production in the proton-nucleus and proton-proton collisions at backward rapidities. Since dileptons do not interact strongly with the final environment, it is relevant to find if the Cronin peak in the backward rapidity region is an initial or final state effect. Also, the nuclear effects are one of our subjects: as it will be seen, these effects are very important and produce visible changes in the nuclear modification ratio at backward rapidities.

We evaluate the dilepton production at backward rapidities using the dipole framework. In this approach in pA collisions and backward rapidities, the nucleus emits a quark which in turn fluctuates into a state of a quark plus a massive photon. The quark interacts with a parton from the proton, freeing the massive photon that subsequently decays into a lepton pair [11]. There are two different diagrams involved (photon emission before and after the interaction) and the dipole cross section arises from the interference of the two bremsstrahlung diagrams, as shown in detail in Ref. [12]. In this approach, the coherence length $l_c \propto 1/x_1$ needs to be larger than the target size, meaning that the interaction time between the projectile quark and the proton must be much shorter than the time of fluctuation of the quark-photon state.

The cross section for the radiation of a virtual photon from a quark (with momentum fraction x_2) of the nucleus scattering off a proton at backward rapidity can be written in a factorized form as [13, 14]:

$$\frac{d\sigma^{DY_{back}}}{dM^2 dy d^2p_T} = \frac{\alpha_{em}^2}{6\pi^3 M^2} \int_0^\infty d\rho W(x_2, \rho, p_T) \sigma_{dip}(x_1, \rho), \tag{1}$$

where p_T is the dilepton transverse momentum, M is the dilepton mass, y is the rapidity, and ρ is the dipole transverse separation. The variables x_1 and x_2 are given by $x_{1,2} = \sqrt{(M^2 + p_T^2)/s} e^{\pm y}$, with s being the squared center of mass energy. As a consequence of backward rapidities ($y < 0$), $x_2 > x_1$. We are investigating dilepton production in pp and pA collisions.

The dipole cross section proposed by Golec-Biernat and Wüsthoff (GBW) [15] is employed here. It has described well the HERA data in both inclusive and diffractive processes for small x.

It is given by:

$$\sigma_{dip}(x_1,\rho) = \sigma_0 \left[1 - \exp\left(-\frac{\rho^2 Q_0^2}{4(x_1/x_0)^\lambda}\right)\right], \tag{2}$$

in which $Q_0^2 = 1$ GeV^2 and $\sigma_0 = 23.03$ mb, $x_0 = 3.04 \times 10^{-4}$ and $\lambda = 0.288$ are fitted parameters.

Based on the dipole approach, the function $W(x_2,\rho,p_T)$ is given by [13]:

$$\begin{aligned} W(x_2,\rho,p_T) = & \int_{x_2}^1 \frac{d\alpha}{\alpha^2} F_2^A(\frac{x_2}{\alpha},M^2) \left\{ [m_q^2\alpha^2 + 2M^2(1-\alpha)^2] \left[\frac{1}{p_T^2+\eta^2} T_1(\rho) - \frac{1}{4\eta} T_2(\rho)\right] \right. \\ & \left. + \; [1+(1-\alpha)^2] \left[\frac{\eta\, p_T}{p_T^2+\eta^2} T_3(\rho) - \frac{1}{2} T_1(\rho) + \frac{\eta}{4} T_2(\rho)\right] \right\}, \end{aligned} \tag{3}$$

where α is the momentum fraction of the quark carried by the virtual photon, $\eta^2 = (1-\alpha)M^2 + \alpha^2 m_q^2$, m_q is the quark mass ($m_q = 0.2$ GeV) and the functions T_i are given by:

$$\begin{aligned} T_1(\rho) &= \frac{\rho}{\alpha} J_0(\frac{p_T\rho}{\alpha}) K_0(\frac{\eta\rho}{\alpha}) \\ T_2(\rho) &= \frac{\rho^2}{\alpha^2} J_0(\frac{p_T\rho}{\alpha}) K_1(\frac{\eta\rho}{\alpha}) \\ T_3(\rho) &= \frac{\rho}{\alpha} J_1(\frac{p_T\rho}{\alpha}) K_1(\frac{\eta\rho}{\alpha}). \end{aligned}$$

Also, the nuclear structure function, given by

$$F_2^A(x,M^2) = \sum_q e_q^2 [x f_q^A(x,M^2) + x f_{\bar{q}}^A(x,M^2)], \tag{4}$$

is considered to take into account the nuclear projectile content. For pp collisions the nuclear structure function $F_2^A(x_2/\alpha,M^2)$ needs to be replaced by the proton structure function $F_2^p(x_2/\alpha,M^2)$.

Two different parametrizations for the nuclear parton distribution functions (nPDFs) are used to obtain F_2^A: one proposed by Eskola, Kolhinen and Salgado (EKS parametrization) [16] and the other, by D. de Florian and R. Sassot (nDS parametrization) [17]. Both provide a global fitting to fixed target experimental results, consider DGLAP equations for Q^2 evolution, and have initial conditions adjusted to describe the DIS in lepton-nucleus collisions and the dilepton production in proton-nucleus collisions. Charge, baryon number, and momentum conservations constrain the parametrizations.

In EKS approach, the nuclear effects are represented simply by a correction factor: $f_q^A(x,Q_0^2) = R_q^A(x,Q_0^2)\, f_q^p(x,Q_0^2)$. A problem of this definition is that the nPDFs are null for $x > 1$, although they should be non-zero for $x < A$. Differently, nDS uses a convolution to obtain nPDFs from free proton PDFs:

$$f_q^A(x,Q_0^2) = \int_x^A \frac{dy}{y} W_q(y,A)\, f_q^p\left(\frac{x}{y},Q_0^2\right), \tag{5}$$

in which the functions $W_i(y,A)$ contain the information about the nuclear effects. For instance, if nuclear effects are disconsidered, $W_q(y,A) = A\delta(1-y)$. We consider the parametrizations at leading-order, since only LO diagrams are employed here. When proton parton distribution functions are needed in this work, the GRV98 parametrization [18] is used.

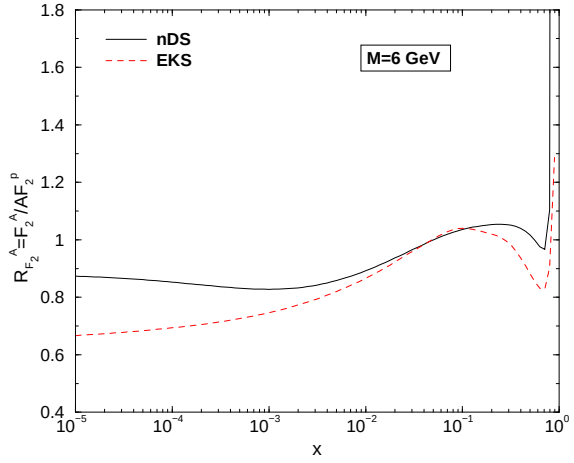

Figure 1: Comparison between EKS and nDS parametrizations for the ratio F_2^A/F_2^p (A=Au) for a dilepton mass (scale) $M = 6$ GeV as a function of the Bjorken x of the nucleus.

In Fig. 1 the ratio F_2^A/F_2^p is presented for both EKS and nDS parametrizations. The figure can be divided in four regions of Bjorken-x [19]. In the Fermi motion region $x \gtrsim 0.8$, $R_{F_2}^A$ is greater than 1 and increases with x. The EMC region $0.3 \lesssim x \lesssim 0.8$ is characterized by $R_{F_2}^A < 1$. The antishadowing region $0.1 \lesssim x \lesssim 0.3$, and the shadowing region $x \lesssim 0.1$ are defined by $R_{F_2}^A > 1$, and $R_{F_2}^A < 1$, respectively. The parametrizations differ most in ECM and shadowing regions, with EKS parametrization getting a lower ratio than nDS.

The use of the dipole approach at backward rapidities presents some limitations. The approach considers an integrated gluon distribution for the nucleus, however, at LHC energies and more central rapidities, the Bjorken x_2 reaches values near 0.002, when this consideration could be questionable. Therefore, finite transverse momentum of the incoming partons could be included in the initial state of the interaction. This could be done considering the k_T factorization approach [20], where the off-shell partonic cross sections are convoluted with k_T unintegrated parton densities $f_a(x,k_T^2,\mu^2)$. Considering Drell-Yan dilepton production, the k_T factorization is investigated in the Ref. [21] and compared with a phenomenological intrinsic k_T approach. In spite of a reasonable data description, the k_T factorization overestimates the data and the intrinsic k_T approach depends on phenomenological parameters (two parameters). For the reasons presented above, we have focused our analysis at backward rapidities and not at more central ones. Moreover, in the dipole approach there is no free parameters and the p_T spectra is finite at low p_T, which justify their use in this work.

Our results are presented through the ratio between pA and pp cross sections:

$$R_{pA} = \frac{d\sigma(pA)}{dp_T^2 dy dM} \Big/ A\frac{d\sigma(pp)}{dp_T^2 dy dM}. \tag{6}$$

This ratio R_{pA} was evaluated at RHIC ($\sqrt{s} = 200$ GeV) and LHC ($\sqrt{s} = 8.8$ TeV) energies and dilepton mass of $M = 6$ GeV. In Figs. 2 and 3 the results are shown in 3D plots for rapidity and p_T spectra, considering EKS and nDS parametrizations. The behavior of the ratio R_{pA} reflects the x_2 dependence of the ratio F_2^A/F_2^p, presented in Fig. 1.

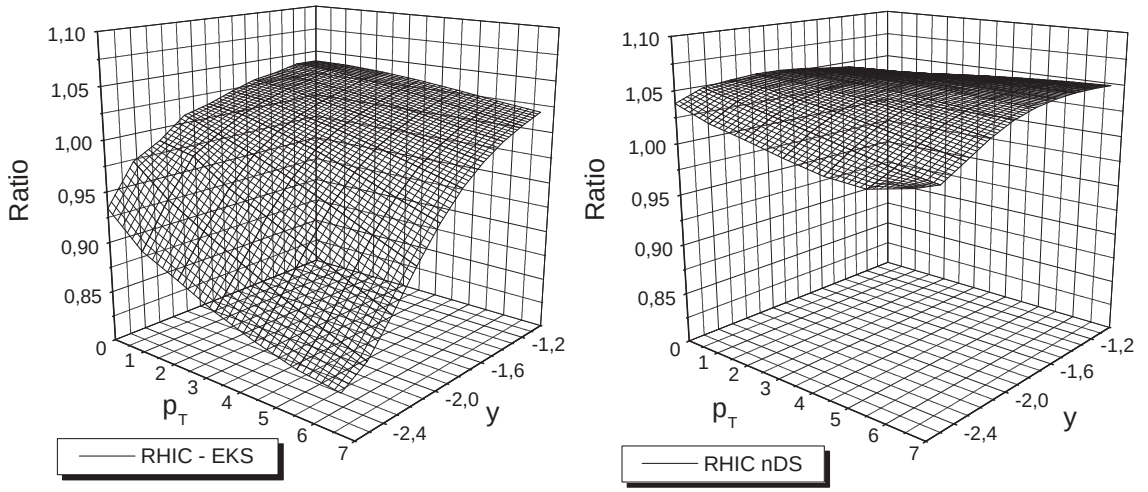

Figure 2: Calculation of R_{pA} for RHIC energies and for EKS and nDS parametrizations.

At RHIC energies, with the EKS parametrization, R_{pA} slowly decreases with p_T and it is seen a suppression of the ratio at very backward rapidities, and large p_T. The nDS parametrization predicts an almost flat behavior. For RHIC energies considering rapidities from -1 to -2.6 and p_T from 1 to 7, the x_2 range is between 0.08 and 0.5, respectively, meaning that for more backward rapidities, partons with larger x_2 are being probed. The nuclear effects that appear in the F_2^A at this x_2 range are mainly due to EMC effect (reduction of the ratio $R_{F_2}^A$ as x_2 increases, see Fig. 1), which provides the reduction of the ratio R_{pA} at lower rapidities in Fig. 2. Concerning the p_T spectra, x_2 increases with p_T, and as the region probed here is related to the EMC effect, the result is a reduction of the ratio R_{pA} as p_T increases. The large suppression of the ratio R_{pA} of the EKS prediction in comparison with the nDS in Fig. 2 is a consequence of the large difference in the $R_{F_2}^A$ predictions of the parametrizations in the EMC effect region.

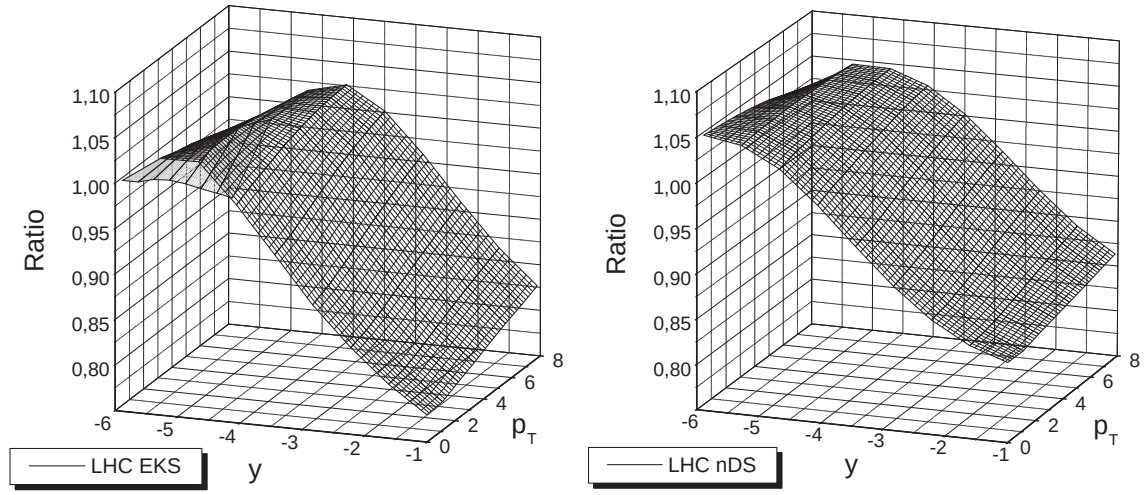

Figure 3: Calculation of R_{pA} for LHC energies and for EKS and nDS parametrizations.

At LHC energies, as the rapidity decreases, the ratio grows, reaches a maximum and de-

creases. The EKS parametrization shows this effect more clearly. The R_{pA} transverse momentum dependence presents two distinct behaviors: for very backward rapidities the ratio decreases as p_T increases and for more central rapidities the ratio R_{pA} increases with p_T. For LHC energies, rapidities from -1 to -6, and p_T from 1 to 7, the x_2 range is between 0.002 and 0.3, respectively. Here we verify that not only large x of the nucleus is been probed, but small x too. The x_2 range probed at LHC provides that shadowing and antishadowing effects are present. The peak at intermediate rapidities is related to the antishadowing effect and the suppression at more central rapidities is related to the shadowing effect. The p_T spectra is more involved since the ratio R_{pA} presents different behaviors. For more backward rapidities the ratio is reduced for large p_T (x_2 in the antishadowing region, near to EMC region). For more central rapidities, the ratio increases for large p_T, since the x_2 is in the shadowing region. As it has been showed in Fig. 1, the EKS parametrization predicts more pronounced antishadowing than the nDS parametrization, which explains the results found here for the ratio R_{pA} at LHC energies.

The previous results for forward rapidities [3] are compared with our results in Fig. 4 for RHIC energies. While at forward rapidities the ratio R_{pA} increases with p_T due to the saturation phenomena, at backward rapidities the ratio R_{pA} decreases with p_T. The distinct behavior of the transverse momentum dependence of R_{pA} is caused by the large x nuclear effects present at backward rapidities.

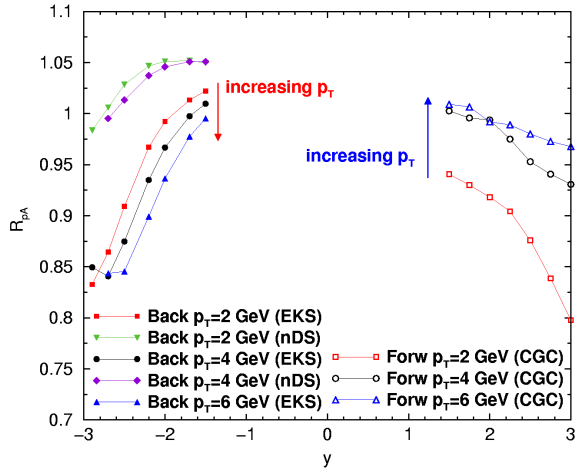

Figure 4: The ratio R_{pA} for dilepton production at backward (EKS and nDS nuclear parametrizations) and forward (CGC predictions [3]) rapidities for RHIC energies.

In conclusion, in our investigation of the nuclear modification ratio R_{pA} for the dilepton production, we have verified a strong dependence on the nuclear effects. This dependence has been explained by the behavior of the nuclear structure function ratio $R^A_{F_2}$. Therefore, the dilepton production at backward rapidities is suitable to understand and quantify the nuclear effects at large and small Bjorken x. Further, the results of hadron production at backward rapidities at RHIC [4] show an increase in the nuclear modification ratio for $1.5 < p_T < 4.0$, in spite of some uncertainties and also discrepancy between methods of data analysis. Since we investigated initial state effects and have not found such increase, our results indicate that the enhancement in the hadron spectra at

backward rapidities could be mainly caused by final state effects. Furthermore, in the forward and backward rapidities comparison, the transverse momentum dependence of R_{pA} is strongly modified at RHIC energies, as different Bjorken x are reached.

References

[1] BRAHMS collaboration, R. Debbe, J. Phys. G 30, S759 (2004). I. Arsene *et al.* The BRAHMS Collaboration, Phys. Rev. Lett. 93, 242303 (2004).

[2] J. Jamal-Jalilian, Y. Kovchegov, Prog. Part. Nucl. Phys. 56, 104 (2006) and references therein.

[3] M.A. Betemps, M.B. Gay Ducati, Phys. Rev. D 70, 116005 (2004); Eur. Phys. J. C 43, 365 (2005); Phys. Lett. B 636, 46 (2006). F. Gelis, J. Jalilian-Marian, Phys. Rev. D 66, 094014 (2002). R. Baier, A.H. Mueller and D. Schiff, Nucl. Phys. A 741, 358 (2004).

[4] S.S. Adler, *et al.* PHENIX Collaboration, Phys. Rev. Lett. 94, 082302 (2005).

[5] V.N. Gribov, L.N. Lipatov, Sov. Journ. Nucl. Phys. 15, 438 (1972). Yu.L. Dokshitzer, Sov. Phys. JETP 46, 641 (1977). G. Altarelli, G. Parisi, Nucl. Phys. B 126, 298 (1977).

[6] E.A. Kuraev, L.N. Lipatov, V.S. Fadin, Phys. Lett. B 60, 50 (1975); Sov. Phys. JETP 44, 443 (1976); Sov. Phys. JETP 45, 199 (1977). I.I. Balitsky, L.N. Lipatov, Sov. J. Nucl. Phys. 28, 822 (1978).

[7] L.V. Gribov, E.M. Levin, M.G. Ryskin, Phys. Rep. 100, 1 (1983). A.H. Mueller, J. Qiu, Nucl. Phys. B 268, 427 (1986).

[8] A.L. Ayala, M.B. Gay Ducati, E.M. Levin, Nucl. Phys. B 493, 305 (1997); Nucl. Phys. B 511, 355 (1998); Phys. Lett. B 388, 188 (1996).

[9] I. Balitsky, Nucl. Phys. B 463, 99 (1996). Y. Kovchegov, Phys. Rev. D 60, 034008 (1999).

[10] J. Jalilian-Marian., A. Kovner, A. Leonidov, H. Weigert, Nucl. Phys. B 504, 415 (1997); Phys. Rev. D 59, 014014 (1999). E. Iancu, A. Leonidov, L.D. McLerran, Nucl. Phys. A 692, 583 (2001); Phys. Lett. B 510, 133 (2001).

[11] B. Z. Kopeliovich, J. Raufeisen, A. V. Tarasov, M. B. Johnson, Phys. Rev. C 67, 014903 (2003).

[12] J. Raufeisen, J.C. Peng, G.C. Nayak, Phys. Rev. D 66, 034024 (2002).

[13] M.A. Betemps, M.B. Gay Ducati, M.V.T. Machado, J. Raufeisen, Phys. Rev. D 67, 114008 (2003).

[14] B.Z. Kopeliovich, In proceedings *Workshop Hirschegg'95: Dynamical Properties of Hadrons in Nuclear Matter.* Ed. by H. Feldmeier and W. Nörenberg, GSI, Darmstadt, p. 102 (1995) [hep-ph/9609385]. S.J. Brodsky, A. Hebecker, E. Quack, Phys. Rev. D 55, 2584 (1997).

[15] K. Golec-Biernat, M. Wüsthoff, Phys. Rev. D 59, 014017 (1999); Phys. Rev. D 60, 114023 (1999).

[16] K.J. Eskola, V.J. Kolhinen, C.A. Salgado, Eur. Phys. J. C 9, 61 (1999). K.J. Eskola, V.J. Kolhinen, P.V. Ruuskanen, Nucl. Phys. B 535, 351 (1998).

[17] D. de Florian, R. Sassot, Phys. Rev. D 69, 074028 (2004).

[18] M. Glück, E. Reya, A. Vogt, Eur. Phys. J. C 5, 461 (1998).

[19] N. Armesto, J. Phys. G: Nucl. Part. Phys. 32, R367-R393 (2006) [hep-ph/0604108].

[20] S. Catani, M. Ciafaloni, F. Hautmann, Phys. Lett. B 242, 97 (1990); Nucl. Phys. B 366, 135 (1991). J. Collins, R. Ellis, Nucl. Phys. B 360, 3 (1991).

[21] O. Linnyk, S. Leupold, U. Mosel, Phys. Rev. D 71, 034009 (2005).